J Musculoskelet Neuronal Interact 2008; 8(4):379-390

Original Article

Hylonome

# Estimation of bone strength from pediatric radiographs of the forearm

**B.A. Varghese, M.E. Miller, T.N. Hangartner**

BioMedical Imaging Laboratory, Wright State University, OH, USA

**Abstract**

**Objective:** Bone strength is a function of both material and architectural properties. However, bone geometry or architecture, which determines the distribution of bone, is an underappreciated determinant of bone strength. The aim of the study was to evaluate the contribution of only architecture to bone strength. **Methods:** We used 2-D (planar) geometric information from radiographs of human radii to construct 3-D finite-element models. To transition from 2-D to 3-D (volume) space, we assumed that all bone cross-sections were elliptical in shape. The finite-element models were subjected to cantilever loading to determine the locations in the bone with the highest propensity to fracture (points of maximum stress). The finite-element-analysis results of the models generated from radiographs of both normal (18) and temporary-brittle-bone-disease (11) infants were subjected to a receiver operating curve analysis. The area under the receiver operating curve was used to evaluate the power of a given bone-strength indicator in segregating the two populations. The actual choice of the material properties (Young's modulus or Poisson's ratio) was not critical for this study, since the finite element analyses were designed to capture the difference in the bone strength of the two populations only based on their architecture. Therefore, the material properties were assumed to be the same in both the normal and TBBD populations. **Results:** The area under the curve of the bending load required to cause fracture among the two populations was 0.82. Other bone-strength indicators, such as average section modulus, cortical thickness and bone length, were associated with an area under the curve of 0.75, 0.73 and 0.63, respectively. **Conclusion:** The results of the finite-element-analysis suggest that the temporary-brittle-bone-disease population has an altered bone geometry, which increases susceptibility to fracture under normal bending loads.

**Keywords:** Radiographs, Finite-element, Temporary Brittle Bone Disease, Fracture

## Introduction

Dual-energy X-ray absorptiometry (DXA) is the most commonly used method to assess bone[1]. The amount of bone, expressed as bone mineral content (BMC) or bone mineral density (BMD), has shown a good correlation with the breaking strength of bone under compression[2,3]. However, this correlation could not be observed under torsion experiments. Several studies showed that, at a continuum level, BMD and Young's modulus are related. Various relationships were established, some linear[4,5] and others power-based[6,7]. The variation in these relationships can be attributed to the diversity of mechanical testing methods and loading conditions used.

The inconsistency of the published observations indicate that BMD alone is not a good indicator of bone strength and that bone architecture - the geometric distribution of bone over the structure - plays an important role. This observation appears valid since BMD tests provide information mainly about how much bone material is present in a specimen, and they mostly overlook the geometry. Recent reports reveal that geometric properties such as moment of inertia and section modulus, i.e., the ratio of a cross-section's moment of inertia to its maximum distance from the neutral axis, enhance the prediction of fracture risk[8-10].

In addition to DXA, plain radiography (PR) and computed tomography (CT) are used as bone imaging techniques[11]. Comparing the three, we observe that both PR and DXA provide two-dimensional (2-D) geometric information of the

The authors have no conflict of interest.

*Corresponding author: Thomas N. Hangartner, Ph.D., BioMedical Imaging Laboratory Wright State University, 3640 Col. Glenn Hwy., 207 Russ Egr. Bldg. Dayton, OH 45435, USA*
*E-mail: thomas.hangartner@wright.edu*

*Accepted 25 September 2008*

bone with loss of the depth information, whereas CT provides full 3-D geometric information as well as quantitative density information if employed with a calibration phantom (quantitative CT, QCT). In contrast to PR, in which BMD cannot be accessed without the introduction of careful calibration and even then only with moderate accuracy, both DXA and QCT are used to quantify bone density. Due to the full 3-D representation of a given bone, QCT would be an ideal modality to assess accurately both the density and cross-sectional geometry simultaneously. However, radiation dose, cost and accessibility often prevent QCT from being used for this purpose.

Our present focus is the assessment of bone strength in infants who present with fractures. In these cases, plain radiographs represent the standard of care for documenting present and possibly previous fractures. Traditionally, the potential for reduced bone strength has been judged based on the radiographic findings of visible darkening of gray levels. This approach is of questionable value for the assessment of small reductions in the amount of bone mass, as there has to be a change in bone mass of about 30-50 percent to visually detect a difference in the gray level in the bone image[12]. Bone mineral loss of less than 30 percent would remain undetected but could cause sufficient reduction in bone strength to facilitate fractures. Despite this limitation of PR, the superior geometric resolution of radiographs compared to DXA and CT might provide a valuable approach to capture accurate bone geometry in 2-D, and thereby assess bone strength.

In the present study, a bone strength assessment method based on radiographs has been developed. We constructed 3-D FE models of the radial bone from anteroposterior (AP) radiographs. To transition from 2-D (area) data to 3-D (volume) data for constructing the FE models, we assumed that all bone cross-sections were elliptical in shape. Once the FE models were constructed, a cantilever loading condition was applied to determine the points of maximum stress, i.e., the locations of bone with the highest propensity to fracture. The fracture loads calculated from radiograph-based FE models were then used as indicators of bone strength.

We tested the method on a pediatric population suffering from temporary brittle bone disease (TBBD). Temporary Brittle Bone Disease (TBBD) is a phenotype of multiple, unexplained fractures in the first year of life and predominantly in the first six months of life. There is usually no other injury such as bruising, subdural hematoma, retinal hemorrhage or other internal injury. The susceptibility to fracture is transient, and there are no other radiographic or biochemical abnormalities noted in the standard evaluation that might suggest an underlying cause[13,14]. Since the symptoms are fleeting after the first six to twelve months, the assessment of bone strength at the time of injury, i.e., when the first fractures occur, becomes increasingly important. This is one of the main reasons why radiographs, which represent the standard of patient care in case of fractures, are usually the only source of imaging data available in TBBD.

## Methods

AP radiographs of 29 infants were studied; 18 infants were known to have normal bone health while the other 11 infants had been diagnosed with TBBD. The radiographs were chosen based on good image quality and an infant age of less than 200 days. The final study population included normal infants ranging from 8-133 days and TBBD infants ranging from 39-183 days. All normal infants included in the study were observed to have normal growth, normal development, no major medical problems and no history of fractures. The TBBD infants suffered from multiple fractures of the ribs and long bones. To be included in the study, TBBD infants needed to have at least one unfractured radius.

To construct 3-D models from 2-D images, the geometry of the third dimension was estimated by using elliptical cross-sections for both the periosteal and endosteal contours of the radius. Circular cross-sections were not considered because they do not provide adequate representation of the cross-sectional geometry of some long bones[15].

To construct an elliptical cross-section, the values of the major and minor diameters and the centre of the ellipse are required. The major diameters are the periosteal and endosteal widths at given positions along the length of the bone (Figure 1). The position of each ellipse in the direction of the major axis is defined by the centre point of the width measurement. Thus, irregularity in cortical thickness along the major axis can be accounted for. Information regarding the minor diameters could not be extracted from the AP radiographs and, hence, were estimated as explained in the next section.

### Regression model for the elliptical aspect ratio of the radius

In the absence of information for the minor diameter, the aspect ratio of the ellipse was measured from cross-sectional images as a function of its location along the length of the bone. Using this information, a bivariate regression model was constructed to identify the aspect ratio of the bone's cross-section along its length for any desired age. The primary datasets used for constructing the regression model were as follows:

1) Computed tomography (CT) sections of the radius of both male and female individuals (age range: 2 months to 65 years).
2) Radiographs showing the AP and mediolateral (ML) views of the radius of children below 5 years of age collected at the Children's Medical Center, Dayton, OH.
3) Cryosections of the Visible Human Model[16,17].
4) Book-based radiographs[18,19].

From CT and cryosection images, the width of the bone corresponding to the major diameter on an AP radiograph was assigned as the major diameter, and the width orthogonal to the major diameter was assigned as the minor diameter.

These measurements, as well as those from the AP and ML radiographs, were associated with age and their relative position along the length of the bone. Plots of the aspect

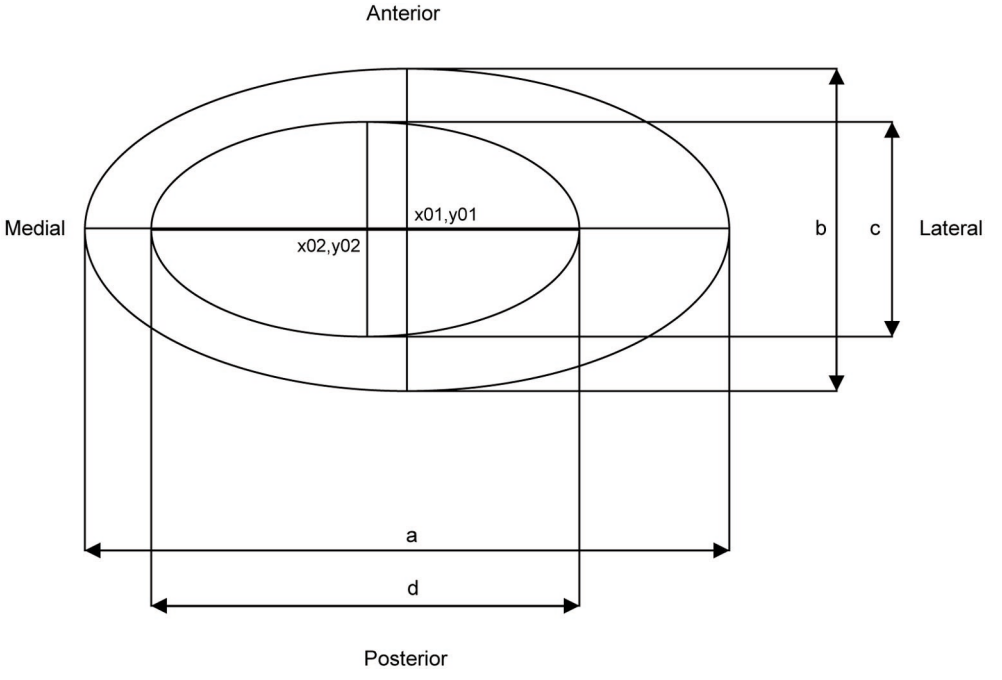


**Figure 1.** The elliptical cross-sectional geometry. The major diameters are 'a' and'd', and the minor diameters are 'b' and 'c'. The two center co-ordinates are x01, y01 and x02, y02, respectively. The points x01 and x02 are the centers of 'a' and'd'.

ratio versus percentage position of individuals falling within the same age group were observed to be comparable; therefore, it was justifiable to combine data based on decades of age. The only exception to this was the infant age group from 0 to 1-year-old. The regression model was then constructed on JMP software (SAS Corporation, Chappell Hill, NC, USA) using the measured aspect ratio versus position along the bone and age. To visually confirm the validity of the model, plots of the aspect ratio versus position along the bone were obtained at the mean age of each age group, using the fitted model, together with the measured data closest to the mean age (Figure 2). The plots show that the constructed bivariate model fits the actual data reasonably well.

Figure 2 also shows that the major-to-minor diameter aspect ratio of the radius is not always 1.0 (circular), rather it varies from 0.5 to 1.0. This suggests that the bone cross-sections are often non-circular and are better approximated by ellipses.

## Construction of ellipses

The procured radiographs were digitized (Howtek iCAD, Inc., Nashua, NH, USA) at the maximum resolution of 12 bits. Due to the jagged shape of the endosteal contours and the relatively low image contrast, the periosteal and endosteal contours were extracted by using the real-time contouring capabilities of ImageJ (http://rsb.info.nih.gov/ij/). This permitted the placement of points along the outer and inner contours of the bone, which were then connected using a spline.

The co-ordinates of all the points forming the endosteal and periosteal spline were stored in a .txt file and imported into Matlab® 6.5 (MathWorks, Natick, MA, USA) These co-ordinates were then used to derive the major diameters of the periosteal and the endosteal ellipses along with their respective centers. The minor diameters were calculated using the regression model. Using the center co-ordinates as well as the major and minor diameters, the endosteal and periosteal ellipses were constructed. The contour co-ordinates of ellipses at a sufficient number of positions along the bone to retain the basic shape of the model were then transferred into the FE modeling software, I-deas® (Integrated Design Engineering Analysis Software, UGS Corp., Plano, Texas, USA).

## Construction of finite-element models in I-deas

The final FE models were constructed from the distal end plate to the proximal end plate of the radius, since the greatest structural contributor to bending strength in long bones is the diaphysis[11]. It was observed from clinical CT images that the medullary cavity extends from about 12 percent of the bone length from the distal end to about 12 percent of the bone length from the proximal end. The medullary cavity contains bone marrow, which was not considered to contribute to the strength of the bone. In the present study, the medullary cavity was modeled as a hollow space within the diaphysis.

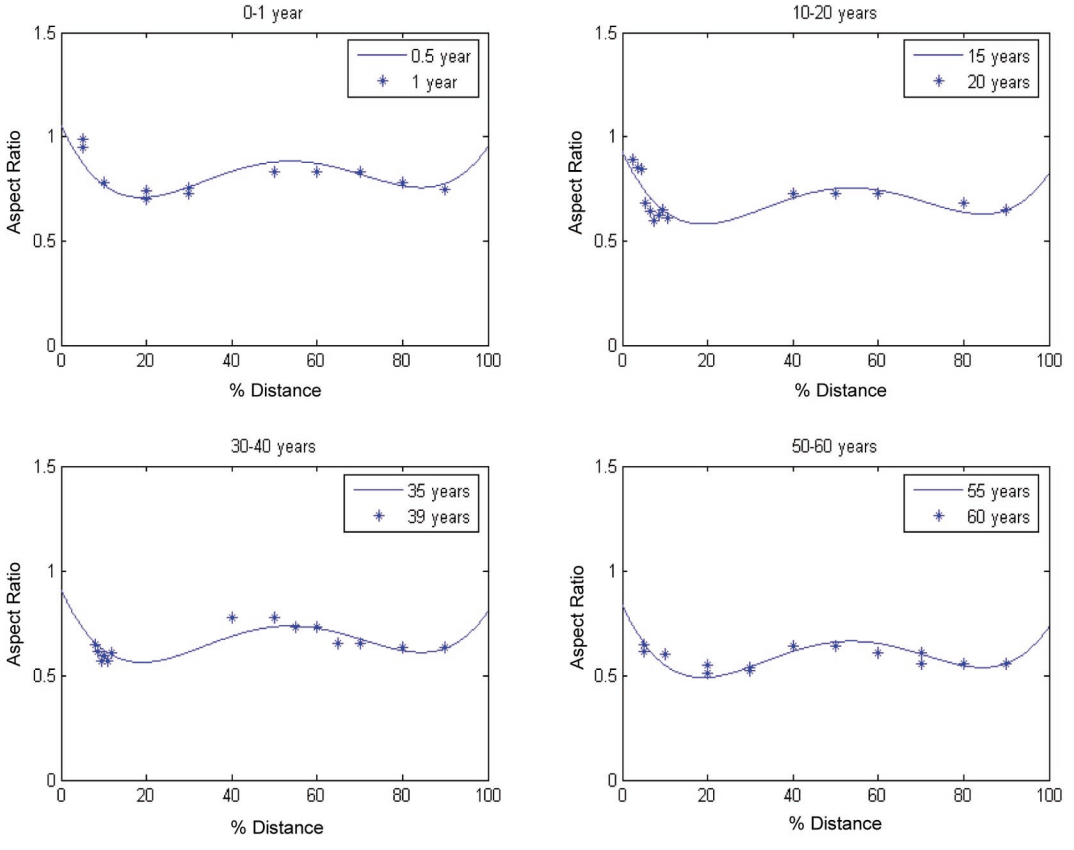


**Figure 2.** Elliptical aspect ratio versus percentage distance of the radius length from the distal end for various age groups using all data sets. In the plot, the continuous line is the aspect ratio obtained using the 2-D equation derived from the regression model for the mean age of each age group. The asterisk values stand for the aspect ratio pertaining to the mean of the measured values within the age group.

## Modeling the bone compartments

From the solid models based on the periosteal and endosteal surfaces, the cortical annulus was constructed by cutting the inner solid (endosteal) from the outer solid (periosteal). Since the bone geometry was obtained from images digitized at 292 dpi, the resulting voxels had a 0.087 mm side length. The cortical region was meshed by breaking the model into finite units. The meshing size of 0.02 units (1 unit=0.087 mm) was obtained after performing a convergence study on the bone models. Ten-node, quadratic, tetrahedral elements were used to capture the curvaceous geometry of the cortex. The material properties of the cortical bone were then introduced; setting $E=4$ GPa and $\upsilon=0.3$, the cortex was meshed and set aside.

The volume described by the endosteal contour was joined with the cortical volume. The endosteal region was then meshed. Ten-node, quadratic, tetrahedral elements were again employed, but in this case the material properties were $E=1$ GPa and $\upsilon=0.3$. At this stage, the bone comprised two regions, the cortical volume filled with trabecular matter in the center. However, the diaphysis does not contain trabecular bone, rather, it houses the medullary cavity. So the lofted medullary cavity was cut out of the endosteal volume from the central 76 percent of the bone length. This led to the formation of the final model in the form of a hollow cortical annulus with 12 percent of the bone length containing trabecular bone at either end.

## Finite-element analysis (FEA)

In reality, long bones, such as the radius, are mostly subjected to bending loads. To capture this loading condition, a cantilever load was used on the bone model. To simplify the modeling process, the load was applied as a point load along the major diameter as opposed to a distributed load.

As mentioned previously, the point of maximum stress is that point on the bone that has the highest propensity to fracture. With increasing loads, the strain at the maximum stress point increases. Other investigators have shown that bone fractures at a strain of 7,000 μstrain[20]. Consequently, the load that creates a maximum local strain of 7,000 μstrain on the bone model was determined.

The maximum strain was calculated by dividing the maxi-

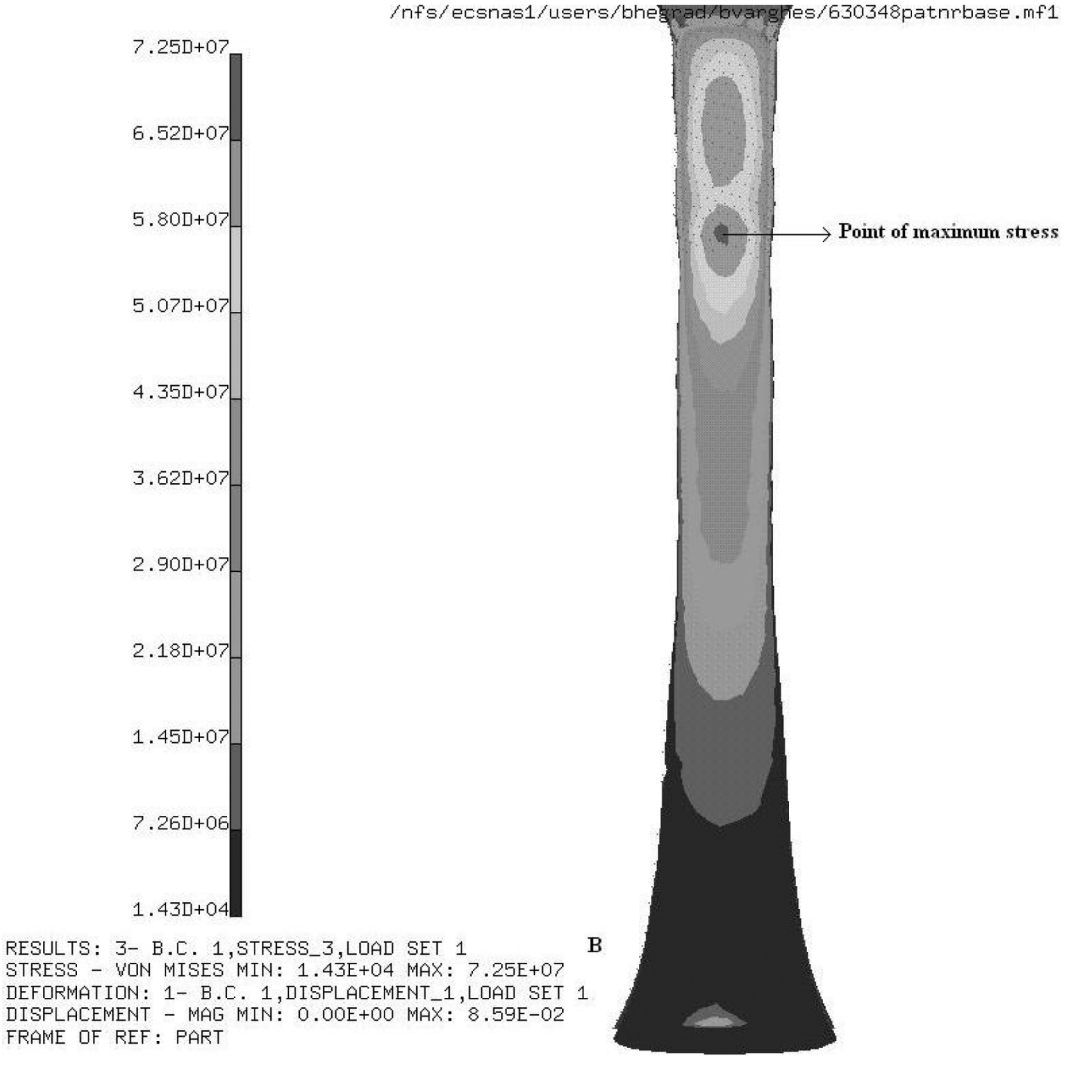


**Figure 3.** Following the FE analysis, the FE model in the figure shows the stress levels as well as the location of the maximum Von Mises stress.

mum calculated stress in the bone by the Young's modulus for cortical bone. The Young's modulus of only the cortical bone was used because the locations of maximum stress in all models were within regions containing cortical bone.

Stress analysis of a cantilever bending scenario, as modeled in this analysis, is usually associated with the maximum principal stress. However, we used the Von Mises stress since the difference to the maximum principal stress values was less than 5 percent and comparatively easier to obtain.

To establish the cantilever loading condition, the displacement of bone in the x, y and z directions was set to zero at the proximal end, and a point load of 111.6 N was applied at the distal end. The value of 111.6 N was obtained for a maximum local strain of 7,000 μstrain from an ancillary study to test model linearity. The study confirmed that strain versus load was linear with an intercept of zero. After solving the simultaneous equations, post-processing through Von Mises stress analysis was carried out (Figure 3). The point on the bone, away from the proximal and distal boundaries, that had the maximum stress was identified; its percentage location along the bone length and the maximum stress value were recorded. The proximal and distal boundaries were not considered for the analysis to avoid boundary effects (high localized stresses due to load application and boundary conditions) based on St. Venant's principle. Sometimes the location of maximum stress appeared in more than one area; in this case the stress value corresponding to the largest region was recorded. Based on the linearity property, the load required to obtain 7,000 μstrain was determined. This procedure was performed on all normal and TBBD bone models. Using model parameters such as bone length, cortical area and total bone area as well as clinical parameters such as age, body weight and height, a receiver operating characteristic (ROC) analysis of the model results were carried out.

| Parameter | Fracture Load | Section Modulus | Cortical Thickness | Bone Length | Weight | Total Width |
|---|---|---|---|---|---|---|
| AUC | 0.82 | 0.75 | 0.73 | 0.62 | 0.57 | 0.54 |

**Table 1.** ROC analysis of the various parameters related to bone strength. The AUC for fracture load was calculated along the minor diameter, average cortical thickness along the major axis.

## Results

Bone is not symmetric; hence, the bone material is not evenly distributed around the neutral axis[21]. So, for the same load, bone can be stronger in a particular direction as compared to another. To test this variability, the fracture-causing loads along the major and minor diameters were determined in separate cantilever bending FE analyses. When bending along the major diameter, the neutral axis was close to the major axis but not coinciding with it due to the variation in cortical thickness along the length of the bone. On the other hand, bending along the minor diameter resulted in the neutral axis coinciding with the minor axis, due to the symmetric distribution of the cortex along the length of the bone. The calculated loads were on average 1.2 times larger along the major axis than along the minor axis, resulting in a correlation coefficient of 0.92.

Since the aim of this study was to find the point where bone is most susceptible to fracture, the fracture loads along the minor diameter were further analyzed. A significant difference ($p<0.001$) between the fracture loads for the normal (mean 53.88 N, standard deviation 16.47 N) and TBBD (mean 38.55 N, standard deviation 8.49 N) populations was observed using an unpaired t-test. This result was representative of the actual differences without taking into consideration other variables such as age and gender.

Due to the small number of TBBD samples (4 males and 7 females), it was not possible to compare the effects of age and gender on the two populations. To find other bone variables that could help distinguish differences between the normal and TBBD populations, ROC analysis was employed. A standard ROC analysis of a given test parameter assesses sensitivity (probability of correctly identifying a diagnosed patient) and specificity (probability of not including a normal person)[22]. The usual ROC plot features the sensitivity on the y-axis and 1-specificity on the x-axis. Depending upon the threshold chosen to segregate the two populations, the test parameter generates a sensitivity and specificity value. The threshold usually varies from the minimum to the maximum value of the test parameter under evaluation.

To assess the performance of the test parameter, the area under the receiver operating characteristic curve (AUC) is employed. The value of the AUC is defined as the probability that, under random selection, a diagnosed person has a different value of the test parameter than a normal person. A test which cannot segregate the two populations would generate a value of 0.5, and a test that perfectly segregates the two populations would generate a value of 1.

ROC values were obtained for several parameters related to bone strength: loading capacity (fracture load), body weight, total bone width, cortical width, bone length and section modulus (Table 1). Considering the AUC, the fracture load had the highest value with 0.82, followed by section modulus (0.75), cortical thickness (0.73) and bone length (0.62). The remaining parameters, body weight and total bone width as measured on the AP radiograph, had lower values. For the cortical thickness and section modulus, five cross-sections above and below the section containing the point of maximum stress were considered and the values averaged.

Since fracture load is a dependent variable, independent variables such as cortical thickness, section modulus and bone length, were used to explain the variation in fracture load across the two diagnostic populations. A plot of section modulus versus bone length reveals that, for a given bone length, the TBBD individuals generally had a lower section modulus at the point of maximum stress than those in the normal group (Figure 4). A similar analysis of cortical thickness showed that, for a given bone length, TBBD individuals had a lower cortical thickness than those in the normal group (Figure 5).

To test the bias of confounding variables such as gender, weight, height, bone length and age on the results, Student t-tests ($p<0.05$) were conducted across the normal and TBBD populations. The t-tests revealed that weight ($p=0.8$), height ($p=0.98$), bone length ($p=0.14$) and age ($p=0.98$) between the two populations were not significantly different from each other. T-tests also ruled out gender-based differences in bone length ($p=0.26$) and age ($p=0.54$) between the two populations. Using multiple regression analysis it was found that the major confounding variables of age, gender, bone length and race explain at best 3% of the variation in fracture load if the disease state, i.e., normal or TBBD, is included, and 8% if it is not included in the model.

## Discussion

Recently, 3-D FE analysis has been extensively used to non-invasively assess bone strength[23,24]. Various methods of generating 3-D FE models have been reported in the literature such as CT-, and microCT-based 3-D FE models, all of which are being evaluated for their precision and accuracy for use in the clinical assessment of bone strength[23-25]. In all these cases

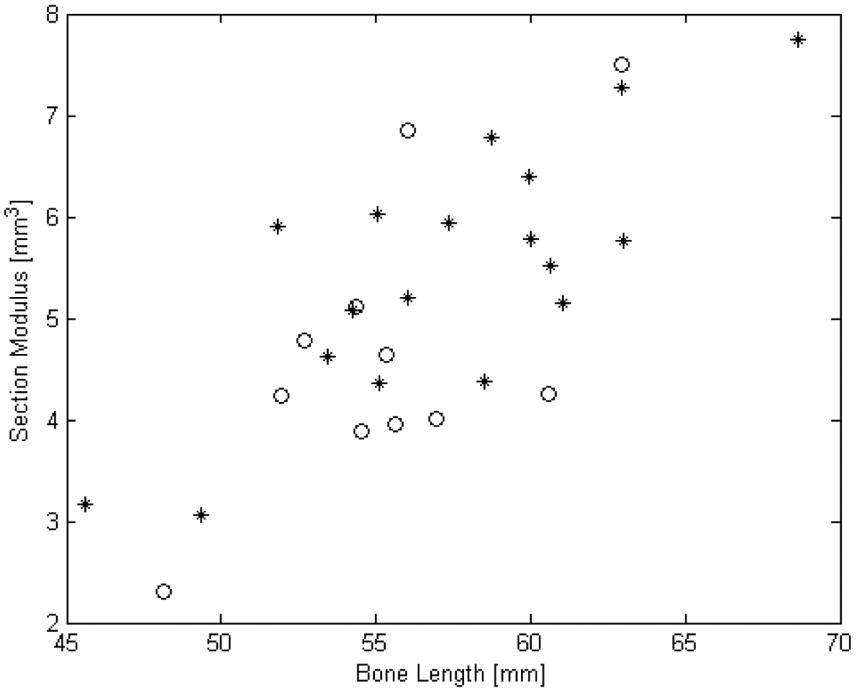


**Figure 4.** Section modulus at the region of maximum stress versus bone length. Bone length was measured from the distal to the proximal end plate. Circle: TBBD Asterisk: Normal.

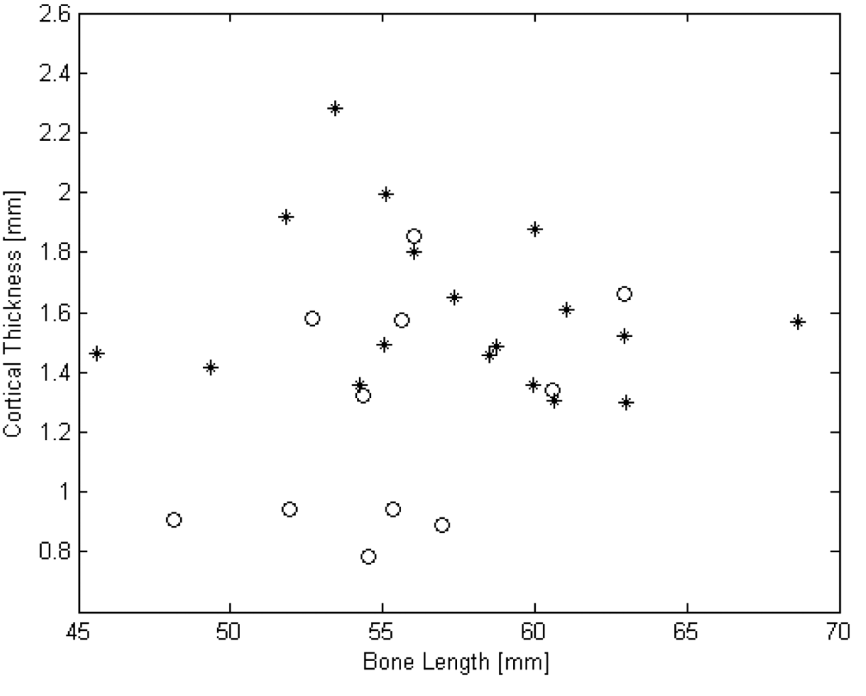


**Figure 5.** Cortical thickness at the region of maximum stress versus bone length. Circle: TBBD Asterisk: Normal.

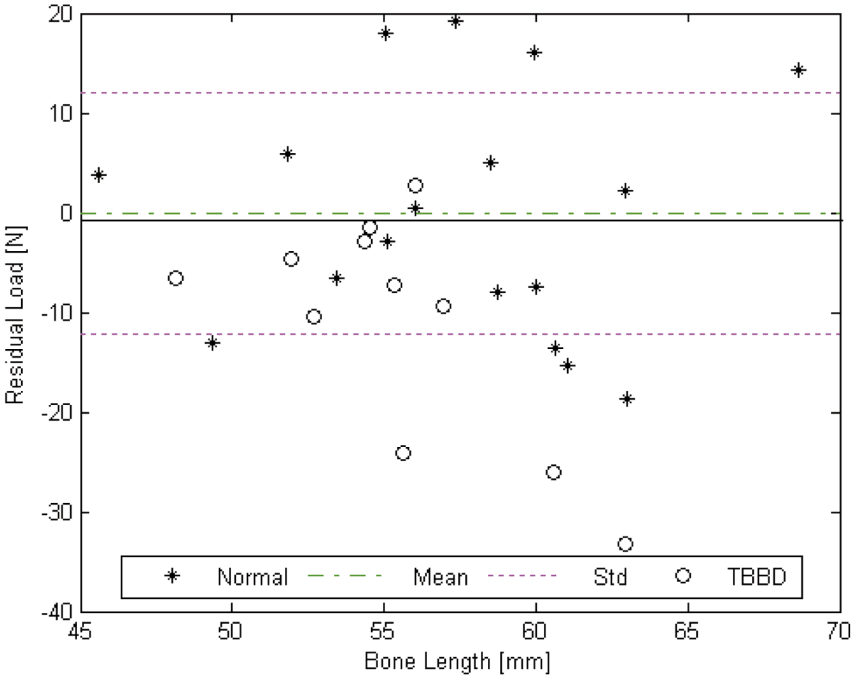


**Figure 6.** Residual of regression of fracture loads along the minor axis versus bone length for normal and TBBD patients. The ±1 standard deviation lines and a horizontal demarcation line just below a residual of zero (-0.1 standard deviation) are also given. Most TBBD cases show values below the horizontal line, but so do about half of the normals (high sensitivity).

cross-sectional data along the length of the bone are available and can be used to extract material and 3-D geometry information. However, here we present a novel procedure for generating 3-D FE models of the radius from projection radiographs. The motivation for developing this technique was to assess pediatric bone strength, where projection radiographs are the standard for imaging and documenting bone fractures. Radiographs are good sources for planar geometry but poor sources for 3-D geometry and material information. Various assumptions regarding the 3-D geometry and material had to be made to construct the 3-D FE model. These assumptions were justified in the current analysis.

Various studies assume bone to be analogous to a beam with circular cross-section, so as to easily implement basic mechanical engineering principles such as beam theory to assess bone strength[11,21]. However, from the analysis of the aspect ratios obtained in this study, it is observed that a circular assumption is not reasonable for the radius, as its true cross-sectional variation along the length of the bone cannot be captured adequately. Similar results have been reported in the femur by Zebaze et al., who state that the circular assumption overestimated the section modulus at the mid-femoral neck by about 51 percent and that the elliptical models reduced the error two- to three-fold[15]. In this study we calculate the depth information required to construct the 3-D geometry from 2-D planar information by assuming the bone cross-sections to be elliptical in shape. Therefore, in the case of AP radiographs, the depths are represented as the minor diameters of the ellipses, which were calculated using the measured major diameter and the aspect ratio-based regression model.

Since radiographs are poor sources for quantifying material parameters (bone density), Young's moduli, as quoted in the literature, were used for both the cortical and trabecular bone. The literature survey revealed a wide range of values for Young's moduli for the normal population, for both cortical (4-27 GPa) and trabecular (1-11 GPa) bone[11,26]. Since the patient population in the present study involved infants below the age of one, the lowest values of either range were chosen. This decision was made based on reports that bone-mineral density and Young's modulus are correlated in adult human bone[27,28]. Unfortunately, similar correlation studies in infants are not available, but it has been reported that infant bones have lower mineral content than normal adult bones[29,30]. An observation of a lower mineral content in infants warrants the use of a lower Young's modulus for both cortical and trabecular bones. The Young's moduli of normal infant's cortical and trabecular bone were, thus, set at 4 GPa and 1 GPa, respectively.

We observed that the ROC results were independent of the exact value of the Young's modulus of cortical and trabecular bone and only dependent on the relative difference between the two. This is because our FE models are linear, and the choice of higher/lower Young's moduli for both cortical and

trabecular bone would proportionately increase/decrease the load-causing fracture. Therefore, provided both moduli are scaled proportionately, the resultant ROC analysis to separate TBBD infants from normals based on the load to fracture will not be affected. Further, since the material constituents of both cortical and trabecular bones are similar on a microscopic level[11], it is reasonable to assume proportional scaling of moduli on a macroscopic level.

Miller et al. have shown, using CT, that TBBD infants have cortical and trabecular bone densities two or more standard deviations below the mean Z-score of age-matched normal infants. Unlike in osteogenesis imperfecta, where the quality or quantity of collagen is abnormal[31,32], studies so far have not shown that the material quality is abnormal in TBBD. Biochemical analyses of the TBBD infants do not show altered collagen or mineralization properties from the normal infants[13]. Therefore, the material properties of both the TBBD and normal infants were assumed to be the same. This ensures that any observed variations in results under a particular loading condition are solely due to differences in architecture and not material.

The ROC results indicate that the altered geometry in TBBD infants predisposes them to fracture under normal loads when compared to the age-matched normal group. Hypothetically, if the material differences between the normal and TBBD infants were taken into consideration in the current models, the lower BMD observed in TBBD infants should cause them to fracture at an even lower load than predicted by geometry alone. This would further strengthen the observation that TBBD infants have altered bone strength compared to age-matched normal infants. It could also be argued that bone geometry compensates for decreased bone material strength. Despite such possible compensation, we find that the bone geometry of TBBD infants results in lower bone strength compared to that of normal infants.

ROC analysis of the FE-model-based bone-strength parameters indicated an AUC value of 0.82 for the load to cause fracture. This is comparable to or better than the AUC values of 0.79, 0.73 and 0.63 recorded for QCT, lateral-DXA and postero-anterior-DXA, respectively, for detecting osteoporotic patients[33]. The replacement of some assumptions in our study with actual measurements (material-based) might further improve the AUC but necessitate a 3-D imaging method. We will need to increase our cohort sizes to ascertain the validity of the calculated AUC with a larger data sample.

In addition to the load to cause fracture, other bone-strength-related parameters such as cortical thickness, section modulus, bone length etc. were evaluated using the ROC analysis and are presented in Table 1. It was observed that the section modulus was the second best strength indicator in the list. The section modulus could serve as a quick and easy estimate of bone strength as compared to load to fracture. However, the exact location of the section modulus on the bone is model-dependent.

The AUC results presented here were obtained using cantilever bending. Bending is the preferred method for investigating the strength of whole long bones when the site of fragility is unknown prior to testing[34]. Bending is also a more physiological type of loading for a long bone compared to pure compression or tension, and these reasons justify the use of cantilever bending in this study. It was observed that the results were loading-dependent. The load required to fracture the bone under torsion was incapable of separating the TBBD population from the normal population (results not shown here). The results under compressive or tensile loading are yet to be evaluated.

Validations of the geometry- and material-based assumptions were not performed; therefore, the accuracy of the FE models was not tested. However, from the results of the FE models, the location of the region of high stress was found to be at the proximal end of the diaphysis about 1-2 cm from the metaphysis. This is a reasonable observation because metaphyseal fractures and occasionally diaphyseal fractures of the extremities are common observations in the long bones of TBBD infants[13,14].

Since bone is asymmetric and its cross-sections vary in shape along its length, bone geometry is better represented in 3-D than 2-D models. This gain in information is associated with an increase in computation time. To estimate the improvement in fracture prediction using 3-D models compared to simple 2-D models, we performed an ROC analysis of the load to cause fracture in 2-D FE models of the bone using identical material and mesh properties as for the 3-D FE models. The 2-D FE models were constructed using the co-ordinates of all points forming the endosteal and periosteal spline and omitting any calculated depth information. The ROC analysis revealed an AUC value of 0.76 which is lower than that obtained from the 3-D model (0.82). This result highlights the potential improvement in the technique when using 3-D FE models generated from volumetric CT data.

There are some potential sources of error that have not been addressed so far. One of the primary sources of error stems from the potential differences in the imaging methods between imaging centers. All our normals were imaged by radiographers at Children's Medical Center, Dayton, Ohio, using the table-top method; i.e., the limb was placed directly on the film cassette. In contrast, radiographs of the TBBD population were part of a collection of radiographs obtained from various imaging centers without information about the imaging conditions. The assumption was made that radiographers in imaging centers globally follow the same pediatric radiography protocol and use the table-top imaging technique for extremities and not the Bucky imaging technique, where the film is placed 5 cm below the table surface. However, if the Bucky technique was used to image the radius, the bones would be magnified by a factor of about 1.1. An ancillary study showed that this would erroneously increase the load required to cause fracture in the TBBD infants by about 2.5 percent. Thus, a correction for the magnification-induced error would reduce the calculated fracture loads and result in an improved separation of the TBBD

population from the normal population.

In general, the radiographs were of poor contrast. Therefore, segmentation was carried out manually by an imaging expert, which may have introduced inconsistencies in the segmentation process. Additionally, errors could have been introduced by improper rotation of the bones. All radiographs were checked for proper rotation of the forearm. The placement of the palm on the film cassette (palm up) and the gap between the proximal and distal styloids of radius and ulna were assessed by a pediatric clinician to ensure that only those radiographs with proper orientation of the bones were included in the study.

Based on the results of this study, we confirm that TBBD infants have altered geometry compared to normal infants, which predisposes them to fractures under normal loads. For a given bone length, TBBD individuals had a lower cortical thickness at the site of maximum stress than those in the normal group (Figure 5). This suggests that the TBBD patients may have a reduced appositional growth and, hence, thinner cortical widths. There have been similar findings in the study of patients with osteogenesis imperfecta[35]. Further, in TBBD infants, genetic, mechanical or chemical factors may cause either a reduced rate of bone formation at the periosteum or an increased rate of bone resorption at the endosteum, both of which lead to the formation of a reduced cortical thickness compared to a normal individual. Although we have established that the TBBD infants have a smaller cortical thickness and section modulus compared to normal infants, we did so at the site of maximum stress, which is identified using the FE model.

### Detecting TBBD in a clinical environment

To use our method clinically, we need to set a threshold for the fracture load to separate TBBD infants from normals. The first step entails fitting a line through the data points obtained for the fracture load of the normal population versus the bone length. Residuals of the load values can be calculated from the fitted line to remove the effect of bone length on the recorded fracture loads (Figure 6). Similarly, the residuals of the TBBD data points can be calculated with respect to the same regression line (Figure 6). In a second step, we draw a demarcation line that segregates the normal population from the TBBD population. Now, an infant with a residual load value above the demarcation line, in this study at -0.1 standard deviation from the regression line of the controls, i.e., -1.4 N, is considered to have normal bone strength, and an infant with a residual load value below the line would have an increased propensity to fracture. The demarcation line was chosen to result in a high sensitivity (minimal false negative results); however, the false positives, i.e., normals with low residual loads, are high at 56 percent. This threshold would be reasonable for a pre-screening method, provided additional tests are conducted to separate the true positives from the false positives. Moreover, validation using larger datasets of normal and TBBD populations having various bone lengths is necessary to establish more trustworthy demarcation lines.

### Alternative method of assessing bone strength

It was seen from the ROC analysis based on FE models in the present study that the calculated section modulus at the points (cross-sections) of maximum stress has a reasonable AUC of 0.75. However, the position of maximum stress is unknown until FE analysis is conducted. To simplify the analysis, a "shortcut" approach could analyze the cross-sectional geometry at a fixed position along the bone. In the present study, the fixed position was chosen as the average of the positions along the length of the bone where maximum stresses were observed over the entire population. This position was calculated to be 17 percent of the bone length from the proximal end. The section modulus calculated at the fixed position using the equation for an elliptical annulus had an AUC of 0.67; using the equation for a circular annulus, the AUC was 0.63. Similar experiments have been conducted by Ruff, where the midshaft and 40 percent locations in the femur and humerus were chosen for measuring the section modulus from radiographs, because they have relatively circular shape at these locations, as observed by CT[36]. Rauch et al. calculated the strength-strain index, which is a bone strength indicator, from pQCT images of the radius, at 4 percent from the distal end[37].

## Summary and conclusions

The contribution of geometry towards bone strength is of great importance. The radiograph-based FE method appears to allow good separation of TBBD infants from normals. The FE analysis is a cost-effective procedure, assuming that only radiographs are used. Future studies, with the aim to determine the sensitivity of various geometric parameters affecting bone strength, need to be performed to better establish the role of bone geometry in assessing the propensity to fracture. Also, the differences in material properties between normals and TBBD cases need to be further evaluated. Eventually, a full-fledged technique can be designed to use both material properties and geometry to model bone strength. Such an approach might provide an improved method for distinguishing fractures caused by child abuse from those caused by TBBD.

*Acknowledgements*

*We would like to thank Ms. Susan McGovern for editorial assistance in preparing this manuscript. BAV acknowledges funding support from Children's Medical Center in Dayton, OH.*

## References

1. Assessment of fracture risk and its application to screening for postmenopausal osteoporosis. Geneva, Switzerland: World Health Organization; 1994.
2. Lin JC, Grampp S, Link T, Kothari M, Newitt D, Felsenberg D, Majumdar S. Fractal analysis of proximal femur radiographs: correlation with biomechanical

properties and bone mineral density. Osteoporos Int 1999;6:516-24.
3. Pienkowski D, McCarter J, Doers T, Maitra R, Monier-Faugere MC, Malluche HH. Bone mineral density compares and contrasts with the biomechanical measurements of canine bone. Bone 1996;19:129S-69.
4. Ducheyne P, Heymans L, Martens M, Aernoudt E, De Meester P, Mulier J. The mechanical behavior of intracondylar cancellous bone of the femur at different loading rates. J Biomech Eng 1977;10:747-62.
5. Martens M, Van Audekercke R, Delport P, De Meester P, Mulier J. The mechanical characteristics of cancellous bone at the upper femoral region. J Biomech Eng 1983;16:971-83.
6. Hodgkinson R, Currey J. Young's modulus, density and material properties in cancellous bone over a large density range. J Mater Sci 1992;3:377-81.
7. Keyak J, Lee I, Skinner H. Correlations between orthogonal mechanical properties and density of trabecular bone: use of different densitometric measures. J Mater Sci 1994;28:1329-36.
8. Mayhew P, Kaptoge S, Loveridge N, Power J, Kroger H, Parker M, Reeve J. Discrimination between cases of hip fracture and controls is improved by hip structural analysis compared to areal bone mineral density. An *ex vivo* study of the femoral neck. Bone 2004;34:352-61.
9. Genant H, Engelke K, Fuerst T, Gluer CC, Grampp S, Harris ST. Noninvasive assessment of bone mineral and structure: state of the art. J Bone Miner Res 1996; 11:707-30.
10. Peacock M, Turner CH, Liu G, Manatunga AK, Timmerman L, Johnston CC Jr. Better discrimination of hip fracture using bone density, geometry, and architecture. Osteoporos Int 1995;5:167-73.
11. Cowin SC. Bone Mechanics. New York: CRC Press; 1989.
12. Harris WH, Heaney RP. Skeletal renewal and metabolic bone disease. N Engl J Med 1969;280:303-11.
13. Miller ME. The lesson of temporary brittle bone disease: all bones are not created equal. Bone 2003;33:466-74.
14. Miller ME, Hangartner TN. Temporary brittle bone disease: association with decreased fetal movement and osteopenia. Calcif Tissue Int 1999;64:137-43.
15. Zebaze RM WF, Juliano BS, Evans A, Seeman E. The femoral neck is ellipsoid: the assumption of circularity or parallelepipedal shape introduces errors in volume and volumetric bone mineral density. J Bone Miner Res 2004;19(Suppl.11):366.
16. Visible Human Project, 1994, Images of digitized cryosections of visible human project (male). Available from http://www.uchsc.edu/sm/chs/browse/browse_m.html. [Accessed on 28/11/05].
17. Visible Human Project, 1995, Images of digitized cryosections of visible human project (female). Available from http://www.uchsc.edu/sm/chs/browse/browse_f.html [Accessed on 28/11/05].
18. Rogers L. Radiology of Skeletal Trauma. New York: Churchill Livingstone; 2002.
19. Browner BD, Jupiter JB, Levine AM, Trafton PG. Skeletal Trauma: Basic Science, Management, and Reconstruction. Philadelphia: Saunders, Elsevier Science; 2003.
20. Pistoia W, Van Rietbergen B, Lochmuller EM, Lill CA, Eckstein F, Ruegsegger P. Estimation of distal radius failure load with micro-finite element analysis models based on three-dimensional peripheral quantitative computed tomography images. Bone 2002;30:842-48.
21. Ohmann JC. Computer software for estimating cross-sectional geometric properties of long bones with concentric and eccentric elliptical models. J Hum Evol 1993;25:217-27.
22. Zweig MH, Campbell G. Receiver-operating characteristic (ROC) plots: a fundamental evaluation tool in clinical medicine. Clin Chem 1993;39:561-77.
23. Keyak JH, Falkinstein Y. Comparison of *in situ* and *in vitro* CT scan-based finite element model predictions of proximal femoral fracture load. Med Eng Phys 2003; 25:781-87.
24. Bessho M, Ohnishi I, Matsuyama J, Matsumoto T, Imai K, Nakamura K. Prediction of strength and strain of the proximal femur by a CT-based finite element method. J Biomech 2007;40:1745-53.
25. Link TM, Sharmila M. Current diagnostic techniques in the evaluation of bone architecture. Curr Osteoporos Rep 2004;2:47-52.
26. Duck FA. Physical Properties of Tissue: A Comprehensive Reference Book. London: Academic Press; 1990.
27. Keyak JH, Rossi SA, Jones KA, Skinner HB. Prediction of femoral fracture load using automated finite element modeling. J Biomech 1998;31:125-33.
28. Keller TS. Predicting compressive mechanical behavior of bone. J Biomech 1994;27:1159-68.
29. Ogle GD, Allen JR, Humphries IRJ, Lu PW, Briody JN, Morley K, Howman-Giles R, Cowell CT. Body-composition assessment by dual-energy X-ray absorptiometry in subjects aged 4-26 years. Am J Clin Nutr 1995;61:746-53.
30. Pierce MC, Bertocci GE, Vogeley E, Moreland MS. Evaluating long bone fractures in children: a biomechanical approach with illustrative cases. Child Abuse Negl 2004;28:505-24.
31. Alman B, Frasca P. Fracture failure mechanisms in patients with osteogenesis imperfecta. J Orthop Res 1987;5:139-43.
32. Kirsch E, Krieg T, Nerlich A, Remberger K, Meinecke P, Kunze D, Müller KP. Compositional analysis of collagen from patients with diverse forms of osteogenesis imperfecta. Calcif Tissue Int 1987;41:11-7.
33. Yu W, Gluer CC, Grampp S, Jergas M, Fuerst T, Wu CY, Lu Y, Fan B, Genant HK. Spinal bone mineral assessment in postmenopausal women: a comparison between dual X-ray absorptiometry and quantitative computed tomography. Osteoporos Int 1995;5:433-9.
34. Beaupied H, Lespessailles E, Benhamou CL. Evaluation

of macrostructural bone biomechanics. Joint Bone Spine 2007;74:233-9.
35. Rauch F, Land C, Cornibert S, Schönau E, Glorieux FH. High and low density in the same bone: a study on children and adolescents with mild osteogenesis imperfecta. Bone 2005;37:634-41.
36. Ruff C. Growth in bone strength, body size, and muscle size in a juvenile longitudinal sample. Bone 2003;33:317-29.
37. Rauch F, Neu C, Manz F, Schönau E, The development of metaphyseal cortex – implications for distal radius fractures during growth. J Bone Miner Res 2001; 16:1547-55.